STRUCTURAL SCIENCE
CRYSTAL ENGINEERING
MATERIALS

Volume 73 (2017)

Supporting information for article:

Structural and Raman spectroscopic characterization of pyroxene-type compounds in the CaCu1−*x*Zn*x*Ge2O6 solid-solution series

Günther J. Redhammer, Gerold Tippelt, Andreas Reyer, Reinhard Gratzl and Andreas Hiederer

S1. More detailed description of structural changes

S1.1. The M2 site

The <Ca-O> bond length is 2.475(3) Å and stays constant within the $P2_1/c$ phase, at the phase change composition a distinct increase is observed up to 2.522(3) Å due to the increase of coordination number from 7 to 8. With increasing Zn^{2+} substitution, <Ca-O> decreases almost linearly to 2.514(3) Å within the $C2/c$ phase. Most of the individual Ca-O bond lengths display similar discontinuous alterations, as sown in Figures 5b – c. Ca-O1A^{vi} decrease within $P2_1/c$ and become shorted at the phase change by 2.25 % (0.054 Å). This correlates well with the increasing M1-O1A^{vi} bond lengths, i.e. there is a movement of the oxygen atoms away from the M1 cations towards the Ca^{2+} atom at the phase change. The Ca-O1B^{iv} bond length has a similar size to Ca-O1A^{vi} and shows the very similar trend, the two bonds become equivalent at the phase change (Ca-O1$^{vi, xi}$ in $C2/c$) and decrease with increasing Zn^{2+} (Fig 5b). The Ca-O2A bond length increases both within the $P2_1/c$ and $C2/c$ phase and is the only one showing no distinct change at the phase change (Fig 5b). The O2A oxygen atom is bonded to Ca, Cu and the Ge of the GeA site. On the contrary, the Ca-O2B^{vii} bond becomes shortened by 7.2 % (0.169 Å) at the phase change. It is the O2B^{vii} atom, which is engaged with the largest bond length alterations also within the M1 octahedron. Within the $C2/c$ phase, the corresponding Ca-O2$^{xiv, xv}$ bonds increase with increasing Zn^{2+} content. It should be recalled that the M1-O2$^{xiv, xv}$ bond lengths decrease at similar extents indicating shifts of the O2 oxygen atoms towards the M1 octahedron, with the M1 coordination polyhedron becoming more regular.

S1.2. The GeA site

The GeA tetrahedron behaves rigid with respect to Cu – Zn substitution, only at the phase change, some small alterations are recognized: the <GeA-O> bond lengths increase somewhat from $P2_1/c$ to $C2/c$, which is mainly due to an increase of the average of the bridging GeA-O distances compared to the non-bridging ones (Fig 6a); associated with this, the difference between the average of bridging and non-bridging Ge-O bonds is larger in the $C2/c$ phase. Also prominent is the change for the O3A-O3A edge, which shortens at the phase change (Fig 6b).

The distortions of the GeA-tetrahedra are small within the $P2_1/c$ phase, however, become larger upon phase change. This is evidenced by any kind of distortion (distortion index, tetrahedral angle variance and tetrahedral quadratic elongation TQE), in Figure 6d, the TQE is shown as an example. Within the C2/c phase the tetrahedral distortion decreases somewhat with increasing Zn content.

S1.3. The GeB site

The GeB site shows the mentioned unique 5-fold coordination. However, taking into account just the four nearest oxygen atoms around GeB in $P2_1/c$, and comparing this as created – very distorted GeB – tetrahedron with the Ge-tetrahedron in C2/c, several marked alterations become evident. The GeB-O3B^{ix} bond gets shortened from 1.892(3) Å in $P2_1/c$ to 1.806(2) Å (-4.7 %) in $C2/c$, while the second bridging GeB-O3B bond increases slightly by 0.2 % from 1.778(3) to 1.782(2) Å. The O3B-O3B^{ix} edge – which is the bridging edge parallel to **c** – is rather short within the $P2_1/c$ phase and increases from 2.605(3) to 2.610(3) with small Zn^{2+} substitutions.

Figure S1 Typical difference thermal analysis curves for the two endmember compositions, collected under normal air conditions.

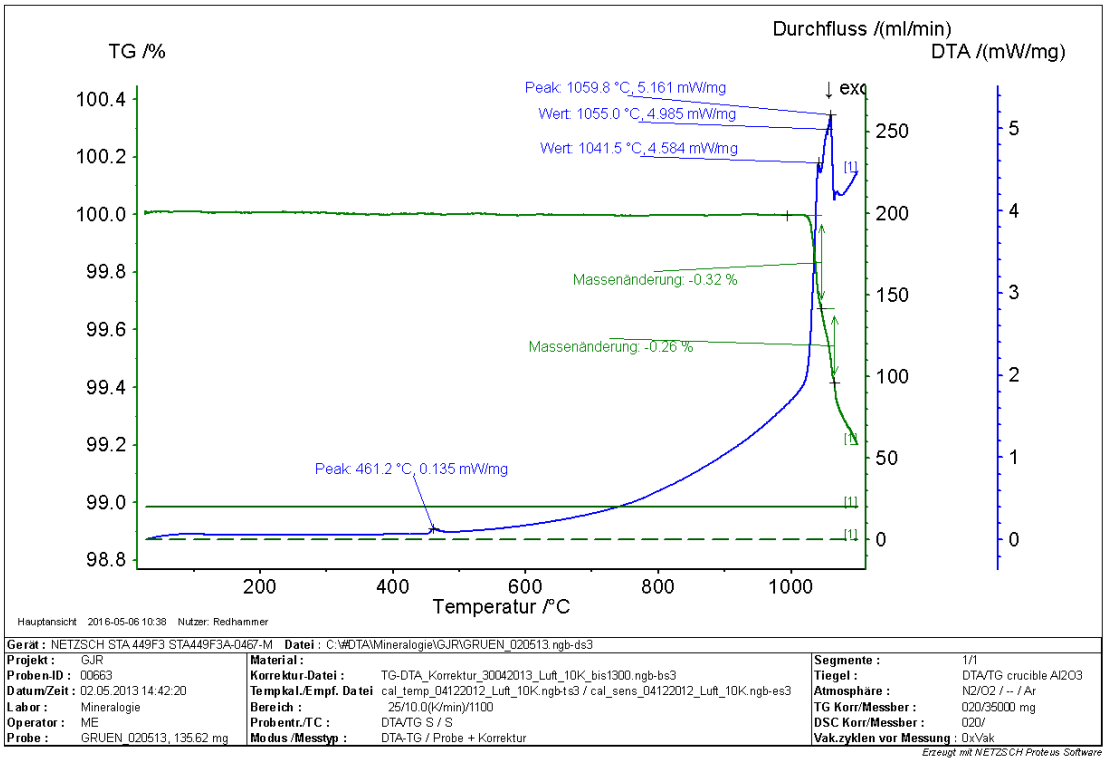

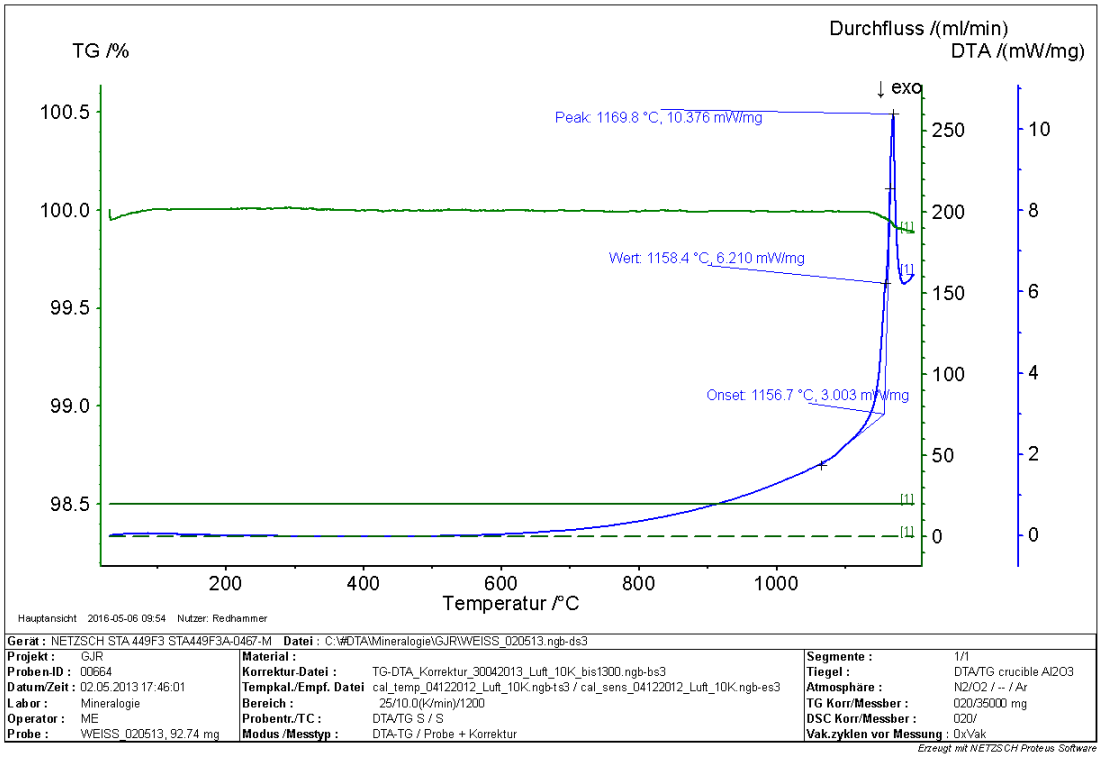

Figure S2 Raman Spectra at 298 K for the whole solid solution series.

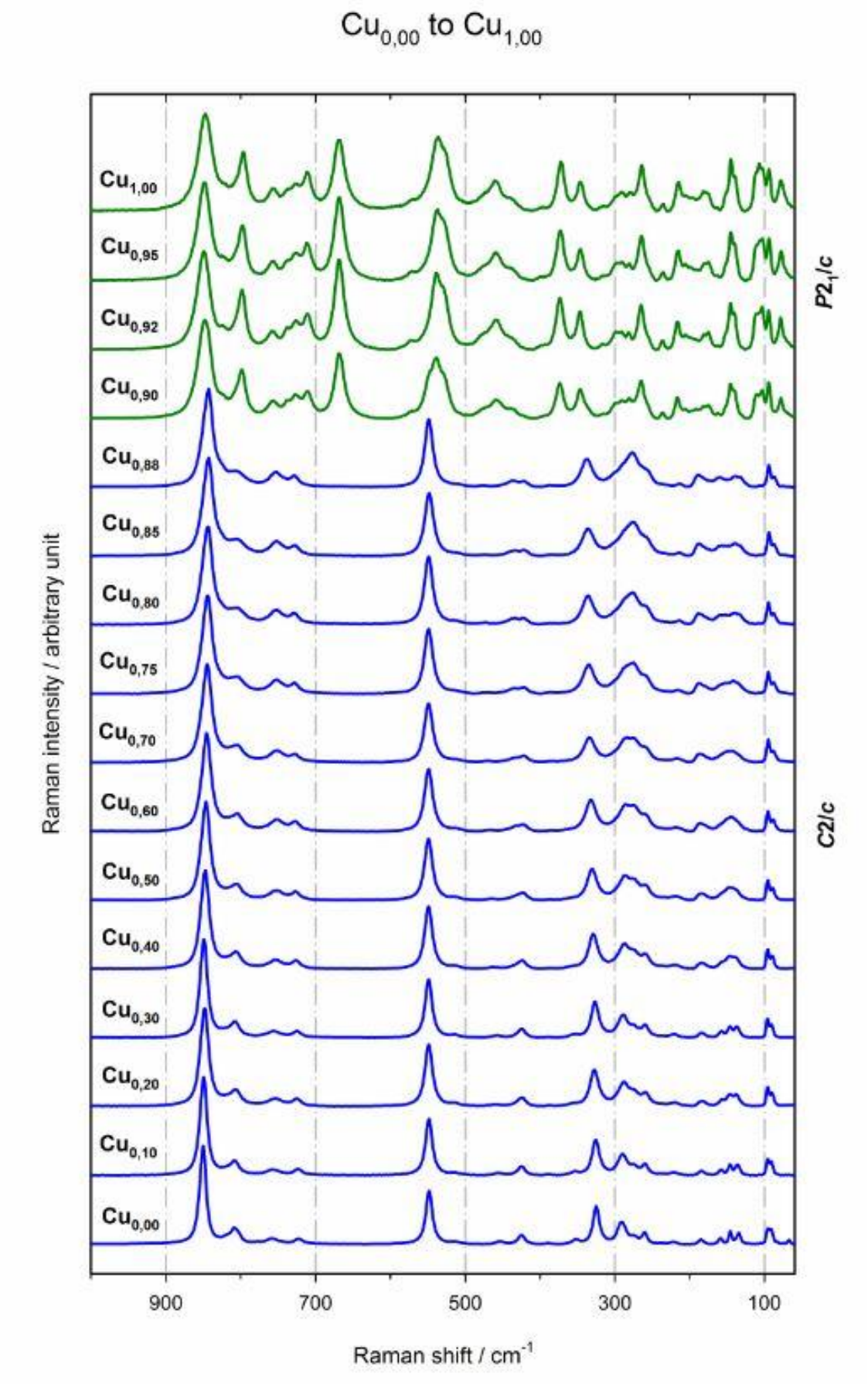

Figure S3 Variation of selected Raman modes as a function of composition within the *C*2/*c* symmetry of the $CaCu_{1-x}Zn_xGe_2O_6$ series.

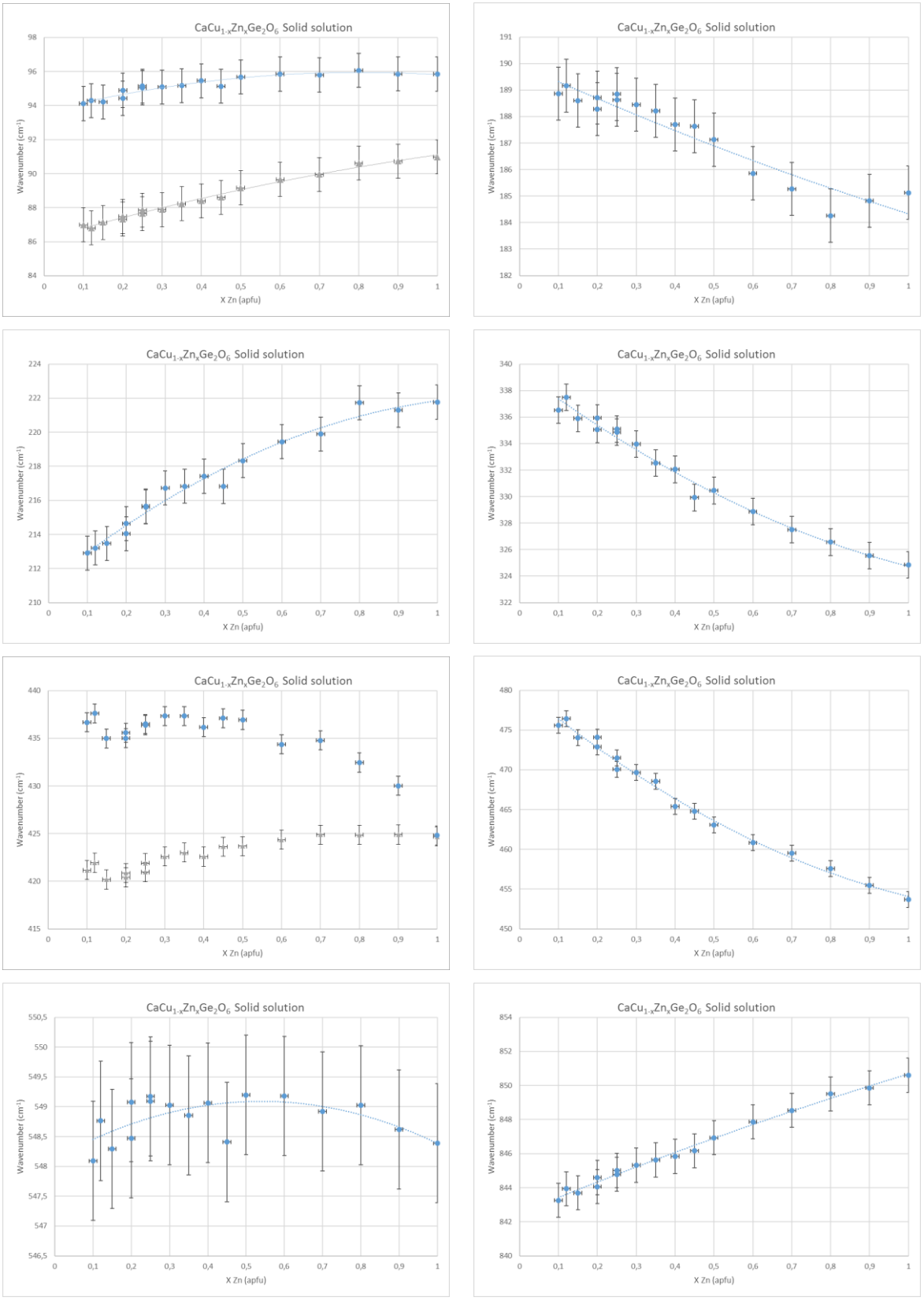

Table S1 Results of the quantitative Rietveld refinements of sintering experiments at different temperatures for three different compositions.

Temperature (K)	1283	1293	1303	1313	1323	1333	1343	1353
$CaCuGe_2O_6$								
*P*2$_1$/*c* Pyroxene								
*C*2/*c* Pyroxene	--	--	--	--	--	--	--	--
$CaGe_2O_5$	--	--	1.9	3.4	9.7	14.3	19.1	30.5
Cu_2O	--	--	--	1.5	1.2	1.6	1.5	1.8
GeO_2	--	--	--	0.4	0.6	0.4	0.4	0.7
$CuGeO_3$	2.3(5)	2.5(5)	2.4(5)	2.5(5)	0.9(5)	--	--	--
$CaCu_{0.95}Zn_{0.05}Ge_2O_6$								
*P*2$_1$/*c* Pyroxene	99.4							
*C*2/*c* Pyroxene	--	--	--			16.3	27.6	25.7
$CaGe_2O_5$	0.2	0.4	0.3	1.3	4.1	13.4	12.8	30.7.6
Cu_2O	--	--	--	--	--	--	0.6	1.2
GeO_2	--	--	--	--	2.1	2.2	1.4	1.6
$CuGeO_3$	0.4	0.7	0.7	0.9	0.4	1.8	2.9	2.1
$CaCu_{0.60}Zn_{0.40}Ge_2O_6$								
*C*2/*c* Pyroxene								
$CaGe_2O_5$	--	--	1.9	3.4	9.7	14.3	19.1	30.5
Cu_2O	--	--	--	1.5	1.2	1.6	1.5	1.8
GeO_2	--	--	--	0.4	0.6	0.4	0.4	0.7
$CuGeO_3$	2.3(5)	2.5(5)	2.4(5)	2.5(5)	0.9(5)	--	--	--

Table S2 Results of strain tensor calculations for the series $CaCu_{1-x}Zn_xGe_2O_6$

x (Zn)	Strain components ε_{ij}				∠ ε3, c	Molar chemical strain $\varepsilon_i/4 * 10^4$			$\varepsilon_1 : \varepsilon_2 : \varepsilon_3$
	ε_{11}	ε_{22}	ε_{33}	ε_{13}		ε_1	ε_2	ε_3	
0.00 - 0.04	0.000681	-0.000414	0.000652	-0.000351	43.82	2.543	-1.034	0.788	1 : -0.41 : 0.31
0.04 - 0.08	0.000732	-0.000414	0.000651	-0.000358	41.77	2.631	-1.035	0.828	1 : -0.39 : 0,31
0.08 - 0.12	0.000784	-0.000414	0.000651	-0.000366	39.84	2.723	-1.035	0.864	1 : -0.38 : 0,32
0.12 : 0.16	0.000836	-0.000414	0.000650	-0.000373	38.03	2.819	-1.035	0.896	1 : -0.37 : 0,32
0.24 – 0.28	0.000176	-0.000469	0.000391	0.000746	40.91	2.593	-1.174	-1.176	1 : -0.45 : -0,45
0.28 – 0.32	0.000172	-0.000466	0.000390	0.000743	40.82	2.580	-1.164	-1.173	1 : -0.45 : -0,45
0.32 – 0.36	0.000168	-0.000462	0.000390	0.000739	40.73	2.566	-1.155	-1.170	1 : -0.45 : -0,46
0.36 – 0.40	0.000165	-0.000458	0.000390	0.000735	40.64	2.554	-1.145	-1.166	1 : -0.45 : -0,46
0.40 – 0.44	0.000161	-0.000454	0.000390	0.000732	40.56	2.540	-1.136	-1.163	1 : -0.45 : -0,46
0.44 – 0.48	0.000157	-0.000450	0.000390	0.000728	40.47	2.528	-1.126	-1.159	1 : -0.45 : -0,46
0.48 – 0.52	0.000154	-0.000447	0.000390	0.000725	40.37	2.515	-1.116	-1.157	1 : -0.44 : -0,46
0.52 – 0.56	0.000150	-0.000443	0.000390	0.000721	40.29	2.502	-1.107	-1.153	1 : -0.44 : -0,46
0.56 - 0.60	0.000147	-0.000439	0.000389	0.000718	40.20	2.489	-1.097	-1.150	1 : -0.44 : -0,46
0.62 – 0.66	0.000143	-0.000435	0.000389	0.000714	40.11	2.477	-1.088	-1.146	1 : -0.44 : -0,46
0.66 -0.70	0.000139	-0.000431	0.000389	0.000711	40.02	2.464	-1.078	-1.143	1 : -0.44 : -0,46
0.70 – 0.74	0.000136	-0.000427	0.000389	0.000707	39.93	2.452	-1.068	-1.139	1 :-0.44 : -0,46
0.74 – 0.78	0.000132	-0.000424	0.000389	0.000703	39.84	2.439	-1.059	-1.136	1 :-0.43 : -0,47
0.78 – 0.82	0.000129	-0.000420	0.000389	0.000700	39.75	2.427	-1.050	-1.132	1 :-0.43 : -0,47
0.82 – 0.86	0.000126	-0.000416	0.000389	0.000696	39.66	2.414	-1.040	-1.129	1 :-0.43 :-0,47
0.86 – 0.90	0.000122	-0.000412	0.000388	0.000693	39.57	2.402	-1.030	-1.125	1 :-0.43 : -0,47
0.90 – 0.94	0.000119	-0.000408	0.000388	0.000689	39.48	2.390	-1.020	-1.122	1 :-0.43 : -0,47
0.94 – 0.98	0.000116	-0.000404	0.000388	0.000686	39.38	2.378	-1.011	-1.118	1 :-0.43 : -0,47
0.98 – 1.00	0.000112	-0.000400	0.000388	0.000682	39.29	2.365	-1.001	-1.115	1 : -0.42 : -0,47

Table S3 Results of Raman mode fitting using Voigt lines of polycrystalline samples of the $CaCu_{1-x}Zn_xGe_2O_6$ solid solution series.

ID	O3 000Cu	RG 010Cu	RG 020Cu	RG 030Cu	RG 040Cu	RG 050Cu	I3 Cu55	RG 060Cu	3 065Cu	RG 070Cu	RG 075Cu	E3 075Cu	RG 080Cu	D3 080Cu	B3 085Cu	CN3_Cu88	B3 090Cu
x (Zn)	1,0	0,9	0,7	0,8	0,6	0,5	0,5	0,4	0,4	0,3	0,3	0,3	0,2	0,2	0,2	0,1	0,1
ν_1	91,0	90,7	90,0	90,6	89,7	89,2	88,6	88,4	88,2	87,9	87,6	87,9	87,5	87,3	87,1	86,8	87,0
ν_2	95,8	95,9	95,8	96,1	95,8	95,7	95,1	95,5	95,2	95,1	95,0	95,1	94,9	94,4	94,2	94,3	94,1
ν_3	134,3	134,5	132,5	133,2	133,4	133,8	133,8	132,5	132,9	132,1	131,9	131,3	132,8	132,4	131,7	131,5	132,2
ν_4	139,2	138,6	137,4	138,3	137,9	139,1	140,4	138,5	139,9	140,1	140,4	139,9	141,4	140,9	139,8	140,0	140,7
ν_5	145,8	146,1	146,4	146,3	146,8	147,0	147,4	145,1	148,9	149,3	148,8	151,0	151,7	151,7	150,0	149,2	150,3
ν_6	158,9	158,2	157,3	157,7	157,4	157,3	157,9	158,9	158,7	158,5	158,0	159,4	160,4	160,2	159,8	160,6	160,1
ν_7	180,3	180,0	179,7	179,7	179,9	180,5	180,7	180,3	180,3	180,3	180,4	181,4	179,8	178,4	179,3	179,4	179,1
ν_8	185,1	184,8	185,3	184,3	185,9	187,1	187,6	187,7	188,2	188,5	188,6	188,9	188,7	188,3	188,6	189,2	188,9
ν_9	221,8	221,3	219,9	221,7	219,4	218,3	216,8	217,4	216,8	216,7	215,6	215,7	214,0	214,6	213,5	213,2	212,9
ν_{10}	237,3	236,7	236,8	236,6	235,9	234,1	233,3	233,5	234,3	234,3	233,6	234,5	232,8	232,9	231,5	231,5	231,8
ν_{11}	260,1	259,6	258,7	259,6	258,8	258,8	257,5	258,4	257,9	258,1	257,2	258,7	258,2	258,0	257,7	256,9	256,7
ν_{12}	274,4	274,2	275,0	274,2	273,7	273,1	274,0	272,9	272,9	272,6	273,3	274,0	274,6	274,0	274,6	276,2	275,5
ν_{13}	290,8	289,9	288,2	289,2	287,6	286,8	286,7	286,5	286,1	285,9	288,2	286,7	286,2	286,4	286,6	289,5	288,4
ν_{14}	324,9	325,5	327,5	326,6	328,9	330,5	329,9	332,1	332,5	334,0	335,1	334,9	335,9	335,1	335,9	337,5	336,5
ν_{15}	352,3	353,6	357,0	355,1	358,8	360,3	362,1	359,9	363,4	366,1	365,8	367,1	368,5	369,1	370,4	372,5	376,7
ν_{16}	390,1	389,6	386,7	387,2	387,3	387,5	388,2	386,2	387,5	385,8	385,8	387,0	386,8	386,1	386,1	386,7	384,8
ν_{17}	424,7	424,9	424,9	424,9	424,4	423,7	423,6	422,6	423,0	422,6	421,9	421,0	420,9	420,4	420,2	421,9	421,2
ν_{18}	424,8	430,0	434,8	432,5	434,4	436,9	437,1	436,2	437,3	437,3	436,4	436,5	435,6	435,0	435,0	437,6	436,7
ν_{19}	453,7	455,5	459,5	457,6	460,8	463,1	464,8	465,4	468,5	469,6	470,1	471,5	474,1	472,9	474,1	476,4	475,6
ν_{20}	514,0	513,7	513,7	513,9	514,0	513,7	513,1	513,0	513,3	512,8	513,9	513,8	513,8	512,4	512,4	513,1	511,9

ν_{21}	548,4	548,6	548,9	549,0	549,2	549,2	548,4	549,1	548,9	549,0	549,1	549,2	549,1	548,5	548,3	548,8	548,1
ν_{22}	722,8	723,8	725,3	725,1	726,4	726,7	726,7	727,3	727,7	727,6	727,8	727,9	728,4	727,3	727,5	728,3	727,7
ν_{23}	758,2	756,8	754,1	755,8	753,7	752,7	752,5	752,3	752,3	751,8	752,4	752,3	752,7	752,1	752,2	753,1	752,2
ν_{24}	807,6	808,0	806,9	807,7	806,2	805,9	805,4	805,5	804,9	804,3	804,9	805,0	804,9	804,4	804,5	805,4	804,6
ν_{25}	820,2	820,9	822,6	822,1	821,8	822,3	822,4	823,1	823,2	823,8	823,6	823,6	823,5	822,9	823,7	824,9	823,8
ν_{26}	850,6	849,9	848,5	849,5	847,9	846,9	846,2	845,8	845,6	845,3	844,8	845,0	844,6	844,1	843,7	843,9	843,3